High Resolution Imaging

10.1 What Is "High Resolution SEM Imaging"? – 148

10.2 Instrumentation Considerations – 148

10.3 Pixel Size, Beam Footprint, and Delocalized Signals – 148

10.4 Secondary Electron Contrast at High Spatial Resolution – 150

10.4.1 SE range Effects Produce Bright Edges (Isolated Edges) – 151

10.4.2 Even More Localized Signal: Edges Which Are Thin Relative to the Beam Range – 152

10.4.3 Too Much of a Good Thing: The Bright Edge Effect Can Hinder Distinguishing Shape – 153

10.4.4 Too Much of a Good Thing: The Bright Edge Effect Hinders Locating the True Position of an Edge for Critical Dimension Metrology – 154

10.5 Achieving High Resolution with Secondary Electrons – 156

10.5.1 Beam Energy Strategies – 156

10.5.2 Improving the SE_1 Signal – 158

10.5.3 Eliminate the Use of SEs Altogether: "Low Loss BSEs" – 161

10.6 Factors That Hinder Achieving High Resolution – 163

10.6.1 Achieving Visibility: The Threshold Contrast – 163

10.6.2 Pathological Specimen Behavior – 163

10.6.3 Pathological Specimen and Instrumentation Behavior – 164

References – 164

J. Goldstein et al., *Scanning Electron Microscopy and X-Ray Microanalysis*,
https://doi.org/10.1007/978-1-4939-6676-9_10

10.1 What Is "High Resolution SEM Imaging"?

"I know high resolution when I see it, but sometimes it doesn't seem to be achievable!"

"High resolution SEM imaging" refers to the capability of discerning fine-scale spatial features of a specimen. Such features may be free-standing objects or structures embedded in a matrix. The definition of "fine-scale" depends on the application, which may involve sub-nanometer features in the most extreme cases. The most important factor determining the limit of spatial resolution is the footprint of the incident beam as it enters the specimen. Depending on the level of performance of the electron optics, the limiting beam diameter can be as small as 1 nm or even finer. However, the ultimate resolution performance is likely to be substantially poorer than the beam footprint and will be determined by one or more of several additional factors: (1) delocalization of the imaging signal, which consists of secondary electrons and/or backscattered electrons, due to the physics of the beam electron – specimen interactions; (2) constraints imposed on the beam size needed to satisfy the Threshold Equation to establish the visibility for the contrast produced by the features of interest; (3) mechanical stability of the SEM; (4) mechanical stability of the specimen mounting; (5) the vacuum environment and specimen cleanliness necessary to avoid contamination of the specimen; (6) degradation of the specimen due to radiation damage; and (7) stray electromagnetic fields in the SEM environment. Recognizing these factors and minimizing or eliminating their impact is critical to achieving optimum high resolution imaging performance. Because achieving satisfactory high resolution SEM often involves operating at the performance limit of the instrument as well as the technique, the experience may vary from one specimen type to another, with different limiting factors manifesting themselves in different situations. Most importantly, because of the limitations on feature visibility imposed by the Threshold Current/Contrast Equation, for a given choice of operating conditions, there will always be a level of feature contrast below which specimen features will not be visible. Thus, there is always a possible "now you see it, now you don't" experience lurking when we seek to operate at the limit of the SEM performance envelope.

10.2 Instrumentation Considerations

High resolution SEM requires that the instrument produce a finely focused, astigmatic beam, in the extreme 1 nm or less in diameter, that carries as much current as possible to maximize contrast visibility. This challenge has been solved by different vendors using a variety of electron optical designs. The electron sources most appropriate to high resolution work are (1) cold field emission, which produces the highest brightness among possible sources (e.g., ~10^9 A/(cm^{2}sr^{-1}) at $E_0 = 20$ keV) but which suffers from emission current instability with a time constant of seconds to minutes and (2) Schottky thermally assisted field emission, which produces high brightness (e.g., ~10^8 A/(cm^{2}sr^{-1}) at $E_0 = 20$ keV) and high stability both over the short term (seconds to minutes) and long term (hours to days).

10.3 Pixel Size, Beam Footprint, and Delocalized Signals

The fundamental step in recording an SEM image is to create a picture element (pixel) by placing the focused beam at a fixed location on the specimen and collecting the signal(s) generated by the beam–specimen interaction over a specific dwell time. The pixel is the smallest unit of information that is recorded in the SEM image. The linear distance between adjacent pixels (the pixel pitch) is the length of edge of the area scanned on the specimen divided by the number of pixels along that edge. As the magnification is increased at fixed pixel number, the area scanned on the specimen decreases and the pixel pitch decreases. Each pixel represents a unique sampling of specimen features and properties, provided that the signal(s) collected is isolated within the area represented by that pixel. "Resolution" means the capability of distinguishing changes in specimen properties between contiguous pixels that represent a fine-scale feature against the adjacent background pixels or against pixels that represent other possibly similar nearby features. Resolution degrades when the signal(s) collected delocalizes out of the area represented by a pixel into the area represented by adjacent pixels so that the signal no longer exclusively samples the pixel of interest. Signal delocalization has two consequences, the loss of spatial specificity and the diminution of the feature contrast, which affects visibility. Thus, when the lateral leakage becomes sufficiently large, the observer will perceive blurring, and less obviously the feature contrast will diminish, possibly falling below the threshold of visibility.

How closely spaced are adjacent pixels of an image? Table 10.1 lists the distance between pixels as a function of the nominal magnification (relative to a 10 x 10-cm display) for a 1000 x 1000 pixel scan. For low magnifications, for example, less than a nominal value of 100×, the large scan fields result in pixel-to-pixel distances that are large enough (pixel pitch >1 μm) to contain nearly all of the possible information-carrying backscattered electrons (BSE) and secondary electrons (SE_1, SE_2, and SE_3) that result from the beam electron–specimen interactions, despite the lateral delocalization that occurs within the interaction volume for the BSE (SE_3) and SE_2 signals.

Table 10.1 reveals that the footprint of a 1-nm focused beam will fit inside a single pixel up to a nominal magnification of 100,000×. However, as discussed in the "Electron Beam–Specimen Interactions" module, the BSE and the SE_2 and SE_3 signals, which are created by the BSE and carry the same spatial information, are subject to substantial lateral delocalization because of the scattering of the beam electrons giving rise to the beam interaction volume, which is beam

Table 10.1 Relationship between nominal magnification and pixel dimension

Nominal magnification (10× 10-cm display)	Edge of scanned area (μm)	Pixel pitch (1000 x 1000-pixel scan)
40×	2500	2.5 μm
100×	1000	1 μm
200×	500	500 nm
400×	250	250 nm
1000×	100	100 nm
2000×	50	50 nm
4000×	25	25 nm
10,000×	10	10 nm
20,000×	5	5 nm
40,000×	2.5	2.5 nm
100,000×	1	1 nm
200,000×	0.5	500 pm
400,000×	0.25	250 pm
1,000,000×	0.1	100 pm

Table 10.2 Diameter of the area at the surface from which 90 % of BSE (SE_3) and SE_2 emerge

E_0	C	Cu	Au
30 keV	11.8 μm	2.6 μm	1.2 μm
20 keV	6.0 μm	1.4 μm	590 nm
10 keV	1.9 μm	410 nm	180 nm
5 keV	590 nm	130 nm	58 nm
2 keV	128 nm	28 nm	12 nm
1 keV	41 nm	8.8 nm	3.9 nm
0.5 keV	12.7 nm	2.8 nm	1.2 nm
0.25 keV	4.0 nm	0.9 nm	0.39 nm
0.1 keV	0.86 nm	0.19 nm	0.08 nm

energy and composition dependent. Table 10.2 gives the diameter of the footprint of the area that contains 90 % of the BSE, SE_2, and SE_3 emission, which is compositionally dependent, as calculated from the cumulative radial spreading plotted in Fig. 2.14. The radial spreading is surprisingly large when compared to the distance between pixels in Table 10.1. For a beam energy of 10 keV, the BSE (SE_3) and SE_2 signals will delocalize out of a single pixel at very low magnifications, approximately 40× for C, 200× for Cu, and 1000× for Au. Even allowing for the fact that the average observer viewing an SEM

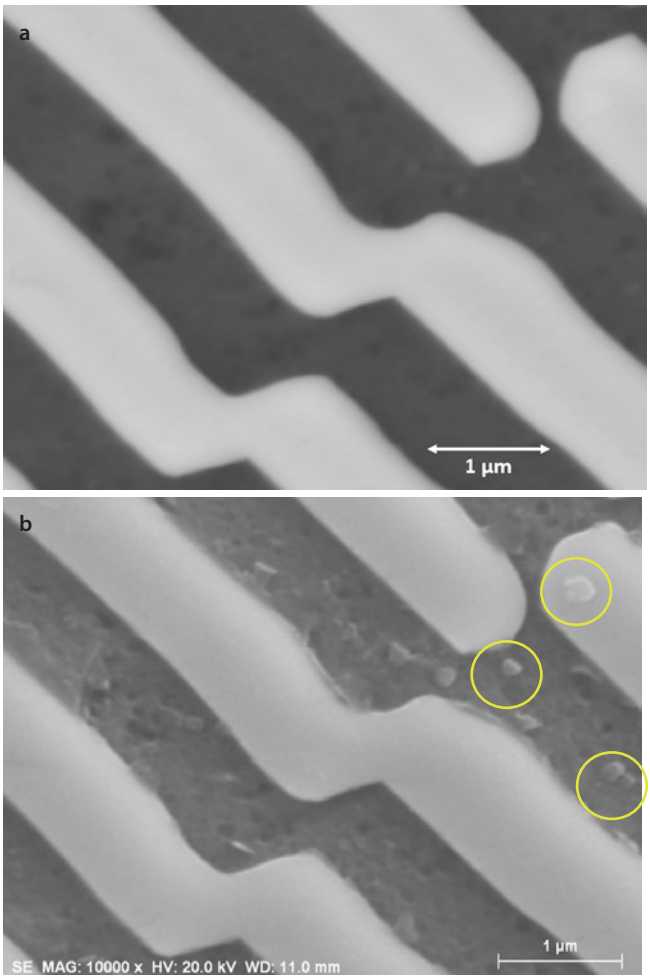

Fig. 10.1 Aluminum-copper eutectic alloy, directionally solidified. The phases are $CuAl_2$ and an Al(Cu) solid solution. Beam energy = 20 keV. **a** Two-segment semiconductor BSE detector, sum mode (A + B). **b** Everhart–Thornley detector(positive bias)

image prepared with a high pixel density scan will only perceive blurring when several pixels effectively overlap, these are surprisingly modest magnification values. Considering that high resolution SEM performance is routinely expected and is apparently delivered, this begs the question: Is such poor resolution actually encountered in practice and why does it not prevent useful high resolution applications of the SEM? Figure 10.1a shows an example of degraded resolution observed in BSE imaging at $E_0 = 20$ keV of what should be nearly atomically sharp interfaces in directionally solidified Al-Cu eutectic. This material contains repeated interfaces (which were carefully aligned to be parallel to the incident beam) between the two phases of the eutectic, $CuAl_2$ intermetallic, and Al(Cu) solid solution. A similar image is shown in Fig. 2.14 with a plot of the BSE signal (recorded with a large solid angle semiconductor detector) across the interface. The BSE signal changes over approximately 300 nm rather than being limited by the beam size, which is approximately 5 nm for this image. The same area is imaged with the Everhart–Thornley detector(positive bias) in Fig. 10.1b and shows finer-scale details, that is, "better resolution." The positively

biased Everhart–Thornley (E–T) detector collects a complex mixture of BSE and SE signals, including a large BSE component (Oatley 1972). The BSE component consists of a relatively small contribution from the BSEs that directly strike the scintillator (because of its small solid angle) but this direct BSE component is augmented by a much larger contribution of indirectly collected BSEs from the relatively abundant SE_2 (produced as all BSEs exit the specimen surface) and SE_3 (created when the BSEs strike the objective lens pole piece and specimen chamber walls). For an intermediate atomic number target such as copper, the SE_2 class created as the BSEs emerge constitutes about 45 % of the total SE signal collected by the E–T(positive bias) detector (Peters 1984, 1985). The SE_3 class from BSE-to-SE conversion at the objective lens pole piece and specimen chamber walls constitutes about 40 % of the total SE intensity. The SE_2 and SE_3, constituting 85 % of the total SE signal, respond to BSE number effects and create most of the atomic number contrast seen in the E–T(positive bias) image. However, the SE_2 and SE_3 are subject to the same lateral delocalization suffered by the BSEs and result in a similar loss of edge resolution. Fortunately for achieving useful high resolution SEM, the E–T (positive bias) detector also collects the SE_1 component (about 15 % of the total SE signal for copper) which is emitted from the footprint of the incident beam. The SE_1 signal component thus retains high resolution spatial information on the scale of the beam, and that information is superimposed on the lower resolution spatial information carried by the BSE, SE_2, and SE_3 signals. Careful inspection of Fig. 10.1b reveals several examples of discrete fine particles which appear in much sharper focus than the boundaries of the Al-Cu eutectic phases. These particles are distinguished by bright edges and uniform interiors and are due in part to the dominance of the SE_1 component that occurs at the edges of structures but which are lost in the pure BSE image of Fig. 10.1a.

10.4 Secondary Electron Contrast at High Spatial Resolution

The secondary electron coefficient responds to changes in the local inclination (topography) of the specimen approximately following a secant function:

$$\delta(\theta) = \delta_0 \sec\theta \tag{10.1}$$

where δ_0 is the secondary electron coefficient at normal beam incidence, i.e., $\theta = 0^\circ$. The contrast between two surfaces at different tilts can be estimated by taking the derivative of Eq. 10.1:

$$\mathrm{d}\delta(\theta) = \delta_0 \sec\theta \tan\theta \,\mathrm{d}\theta \tag{10.2}$$

The contrast for a small change in tilt angle $\mathrm{d}\theta$ is then

$$C \sim \mathrm{d}\delta(\theta)/\delta(\theta) = \delta_0 \sec\theta \tan\theta \,\mathrm{d}\theta / \delta_0 \sec\theta = \tan\theta \,\mathrm{d}\theta \tag{10.3}$$

As the local tilt angle increases, the contrast between two adjacent planar surfaces with a small difference in tilt angle, $\mathrm{d}\theta$, increases as the average tilt angle, θ, increases, as shown in Fig. 10.2 for surfaces with a difference in tilt of $\mathrm{d}\theta = 1^\circ, 5^\circ$

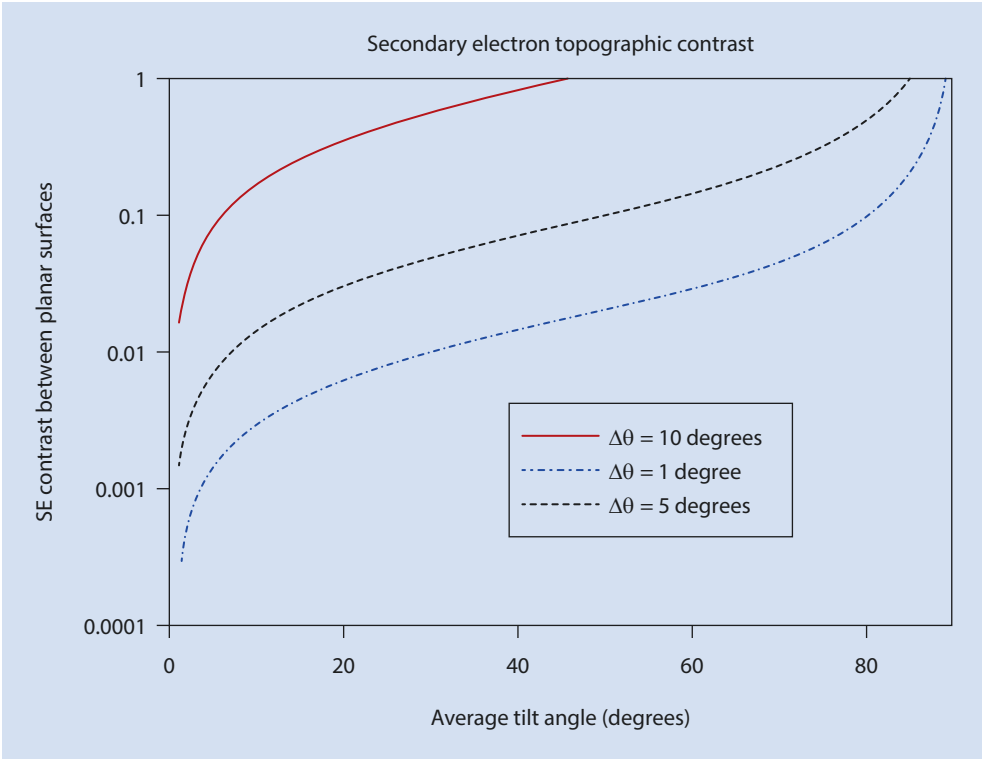

Fig. 10.2 Plot of secondary electron topographic contrast between two flat surfaces with a difference in tilt angle of 1°, 5°, and 10°

and 10°. Superimposed on this broad scale secondary electron topographic contrast are strong sources of contrast associated with situations where the range of SEs dominates leading to enhanced SE escape:

1. When the beam strikes nearly tangentially, that is, grazing incidence when θ approaches 90° and sec θ reaches very high values, as the beam travels near the surface and a high SE signal is produced, an effect that is seen in the calculated contrast at high tilt angles in ◘ Figs. 10.2 and 10.3 show an example of a group of particles imaged with an E–T(positive bias) detector. High SE signals occur where the beam strikes the edges of the particles at grazing incidence, compared to the interior of the particles where the incidence angle is more nearly normal.
2. At feature edges, especially edges that are thin compared to the primary electron range. These mechanisms result in a very noticeable "bright edge effect."

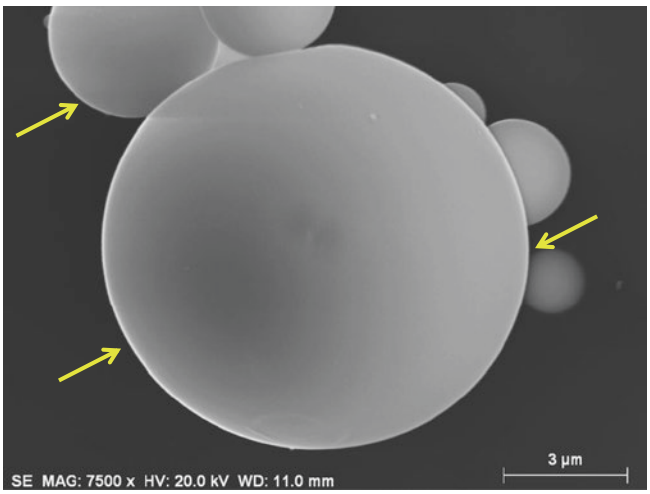

◘ **Fig. 10.3** SEM image of SRM 470 (Glass K -411) micro-particles prepared with an Everhart–Thornley detector(positive bias) and $E_0 = 20$ keV. Note bright edges where the beam strikes tangentially

10.4.1 SE Range Effects Produce Bright Edges (Isolated Edges)

Because of their extremely low kinetic energy of a few kiloelectronvolts, SEs have a short range of travel in a solid and thus can only escape from a shallow depth. The mean escape depth (SE range) is approximately 10 nm for a conductor. When the beam is located in bulk material well away from edges, as shown schematically in ◘ Fig. 10.4, the surface area from which SEs can escape is effectively constant as the beam is scanned, and the SE emission (SE_1, SE_2, and SE_2) is thus constant and equal to the bulk SE coefficient appropriate to the target material at the local inclination angle. However, when the beam approaches an edge of a feature, such as the vertical wall shown in ◘ Fig. 10.4, the escape of SEs is enhanced by the proximity of additional surface area that lies within the SE escape range. As the incident beam travels nearly parallel to the vertical face, the proximity of the surface along an extended portion of the beam path further enhances the escape of SEs, resulting in a very large

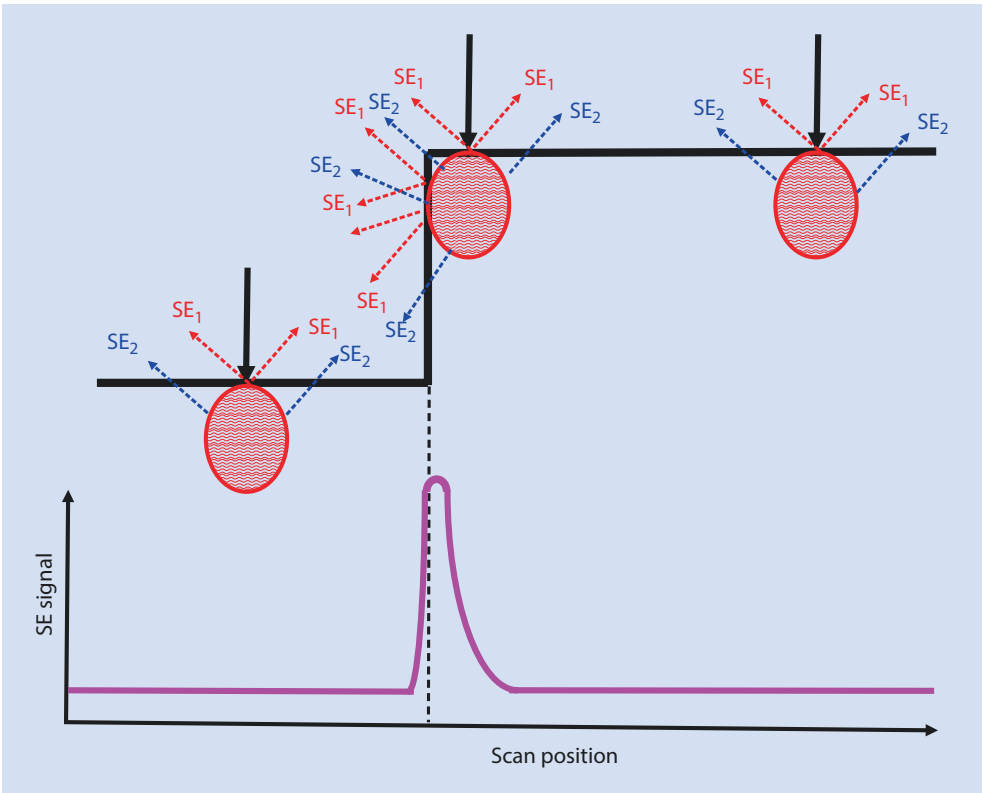

◘ **Fig. 10.4** Schematic diagram showing behavior of BSE and SE signals as the beam approaches a vertical edge

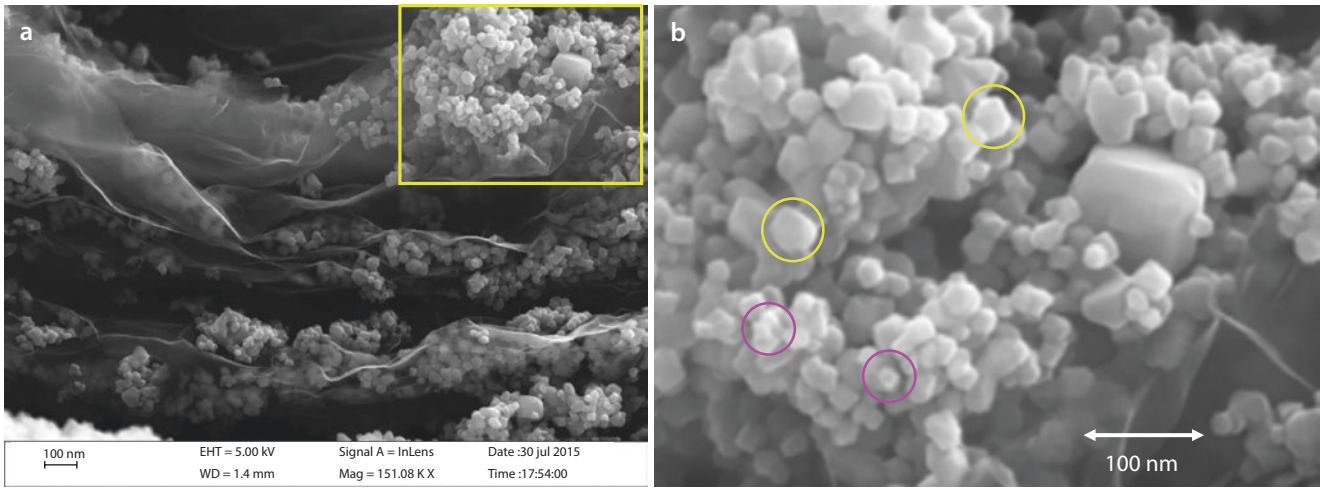

Fig. 10.5 **a** SEM image at $E_0 = 5$ keV of TiO_2 particles using a through-the-lens detector for SE_1 and SE_2 (Bar = 100 nm). **b** Note bright edge effects and convergence of bright edges for the smallest particles (Example courtesy John Notte, Zeiss)

excess of SEs compared to the bulk interior. In addition, there will be enhanced escape of BSEs near the edge, and these BSEs will likely strike other nearby specimen and instrument surfaces, producing even more SEs. All of the signals collected when the beam is placed at a given scan location are assigned to that location in the image no matter where on the specimen or SEM chamber those signals are generated. The apparent SE emission coefficient when the beam is placed near an edge is thus greatly increased over the bulk interior value, often by a factor of two to ten depending on the exact geometric circumstances. The edges of an object will appear very bright relative to the interior of the object, as shown in Fig. 10.5 (e.g., objects in yellow circles in Fig. 10.5b) for particles of TiO_2. Since the edges are often the most important factor in defining a feature, a contrast mechanism that produces such an enhanced edge signal compared to bulk is a significant advantage. This is especially true considering the limitations that are imposed on high resolution performance by the demands of the Threshold Current/Contrast Equation, as discussed below.

10.4.2 Even More Localized Signal: Edges Which Are Thin Relative to the Beam Range

The enhanced SE escape near an edge shown in Fig. 10.4 is further increased when the beam approaches a feature edge that is thin enough for penetration of the beam electrons. As shown schematically in Fig. 10.6, not only are additional SEs generated as the beam electrons emerge as "BSEs" through the bottom and sides of the thin edge

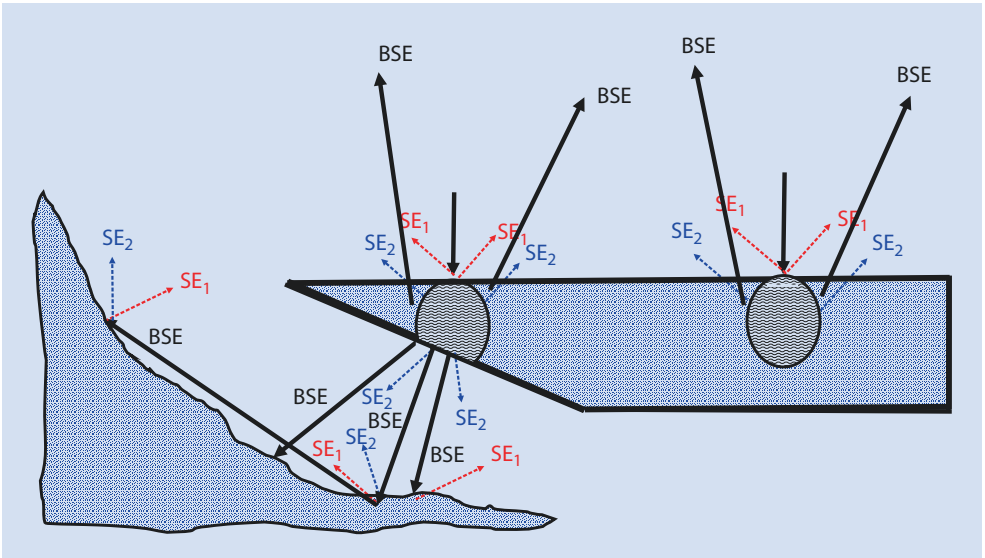

Fig. 10.6 Schematic diagram of the enhanced BSE and SE production at an edge thin enough for beam penetration. BSEs may strike multiple surfaces, creating several generations of SEs

structure, but these energetic BSEs will continue to travel, backscattering off other nearby specimen surfaces and the SEM lens and chamber walls, producing additional generations of SEs at each surface they strike. These additional SEs will be collected with significant efficiency by the E–T (positive bias) detector and assigned to each pixel as the beam approaches the edge, further increasing the signal at a thin edge relative to the interior and thus increasing the contrast of edges.

10.4.3 Too Much of a Good Thing: The Bright Edge Effect Can Hinder Distinguishing Shape

As the dimensions of a free-standing object such as a particle or the diameter of a fiber approach the secondary electron escape length, the bright edge effects from two or more edges will converge, as shown schematically in Fig. 10.7 and in the image of TiO2 particles (e.g., objects in magenta circles)

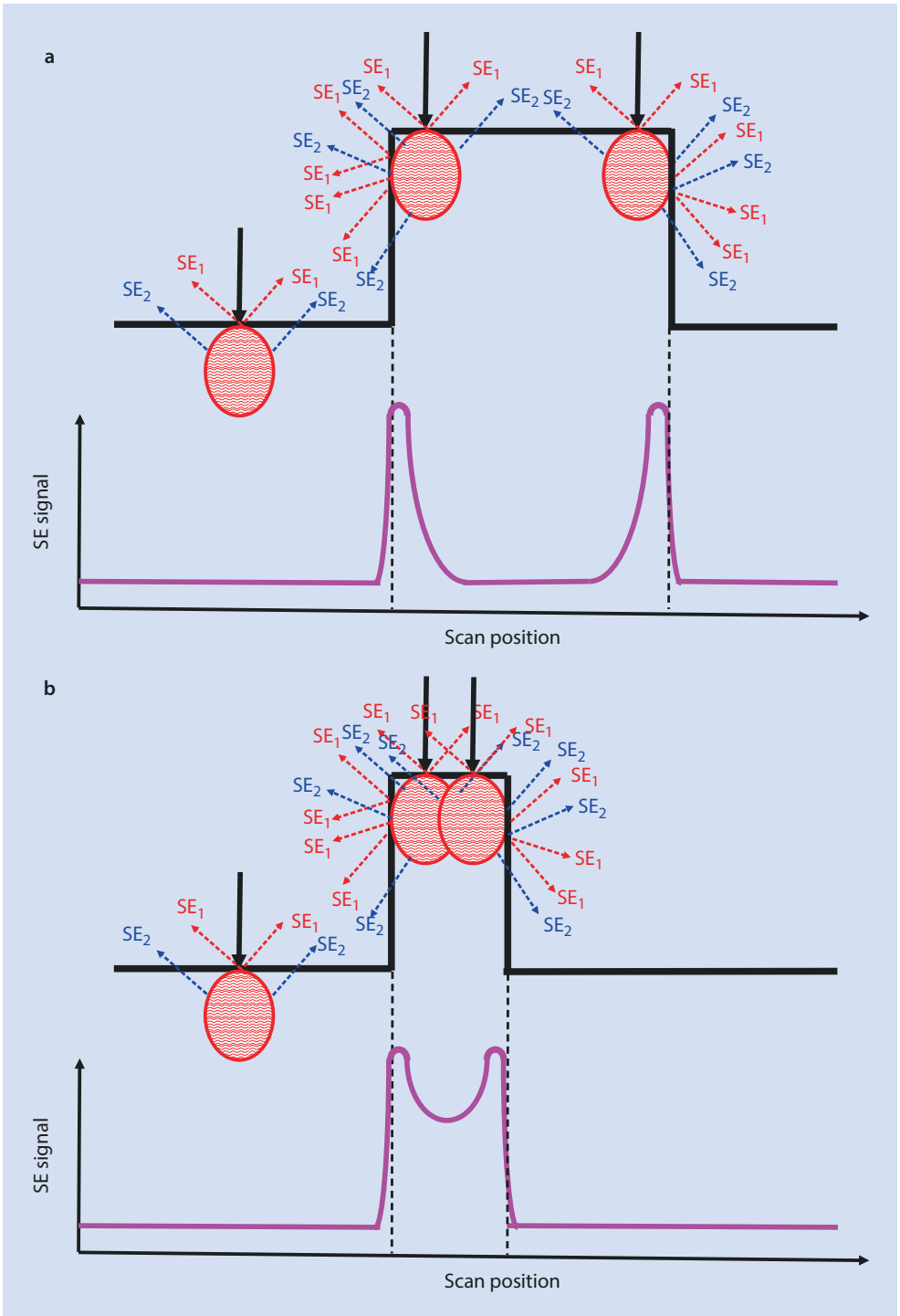

Fig. 10.7 Convergence of bright edges as feature dimensions approach the SE escape distance. **a** Object edges separated by several multiples of the SE escape distance so that edge effects are distinct; **b** object edges sufficiently close for edge effects to begin to merge

shown in Fig. 10.5b. While the object will appear in high contrast as a very bright feature against the background, making it relatively easy to detect, as an object decreases in size it becomes difficult and eventually impossible to discern the true shape of an equiaxed object and to accurately measure its dimensions.

10.4.4 Too Much of a Good Thing: The Bright Edge Effect Hinders Locating the True Position of an Edge for Critical Dimension Metrology

While the enhanced SE escape at an edge is a great advantage in visualizing the presence of an edge, the extreme signal excursion and its rapid change with beam position make it difficult to locate the absolute position of the edge within the SE range, which can span 10 nm or even more for insulating materials. For advanced metrology applications such as semiconductor manufacturing critical dimension measurements where nanometer to sub-nanometer accuracy is required, detailed Monte Carlo modeling, as shown in Fig. 10.8, of the beam electron, backscattered electron, and secondary electron trajectories as influenced by the specific geometry of the edge, is needed to deconvolve the measured signal profile as a function of scan position so as to recover the best estimate of the true edge location and object shape (NIST JMONSEL: Villarrubia et al. 2015). An example of an SEM signal profile across a structure and the shape recovered after deconvolution through modeling is shown in Fig. 10.9. An application of this approach is shown in Fig. 10.10, where a three-dimensional photoresist line was first imaged in a top-down SEM view (Fig. 10.10a). Monte Carlo modeling applied to the signal profiles obtained from the top-down view enabled a best fit estimate of the shape and dimensions of the line. The structure was subsequently cross-sectioned by ion beam milling to produce the SEM view shown in Fig. 10.10b. The best estimate of the structure obtained from the top-down imaging and modeling (red trace) is shown superimposed on the direct image of the cross-section edges (blue trace), showing excellent correspondence with this approach.

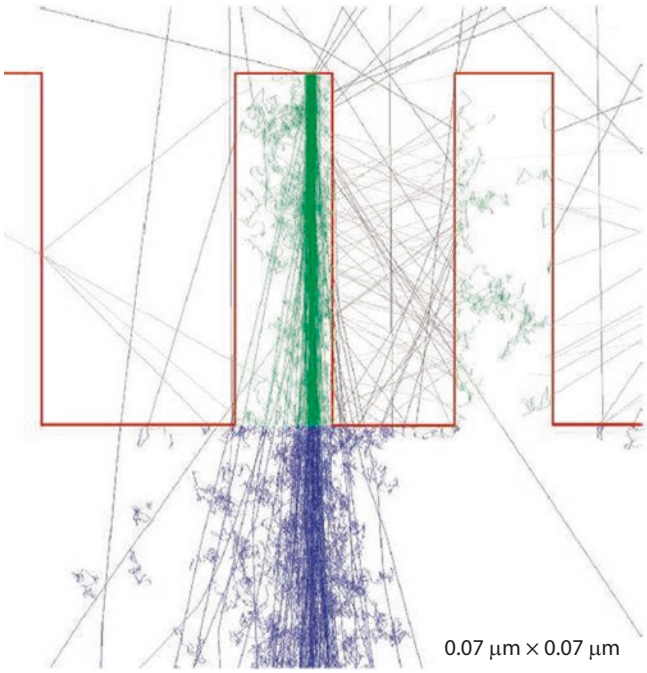

Fig. 10.8 Monte Carlo electron trajectory simulation of complex interactions at line-width structures as calculated with the J-MONSEL code (Villarrubia et al. 2015)

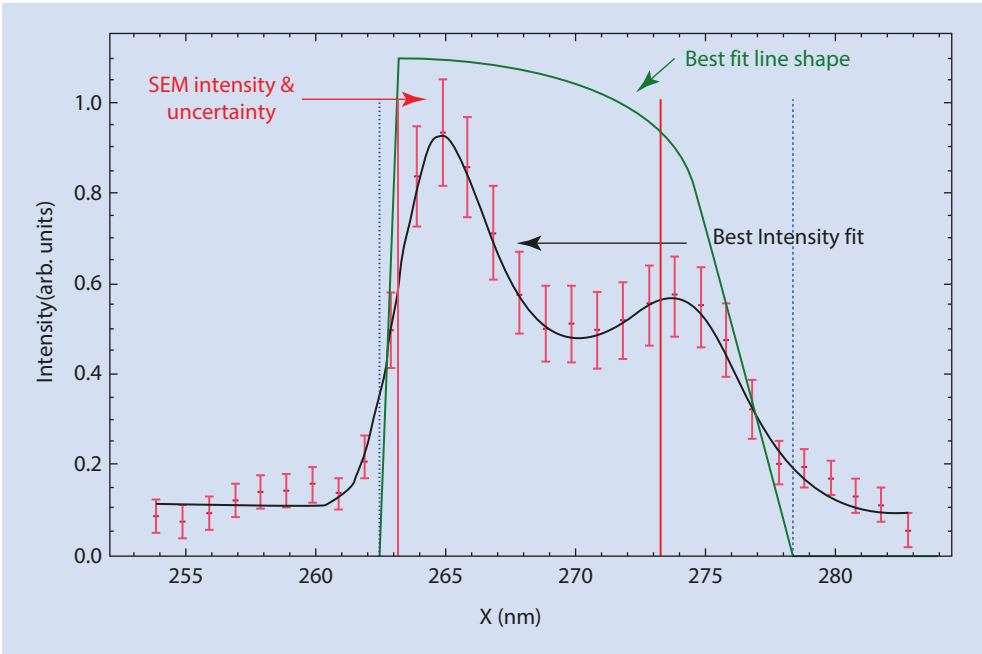

Fig. 10.9 Application of J-MONSEL Monte Carlo simulation to measured SEM profile data and the estimated shape that best fits the data (Villarrubia et al. 2015)

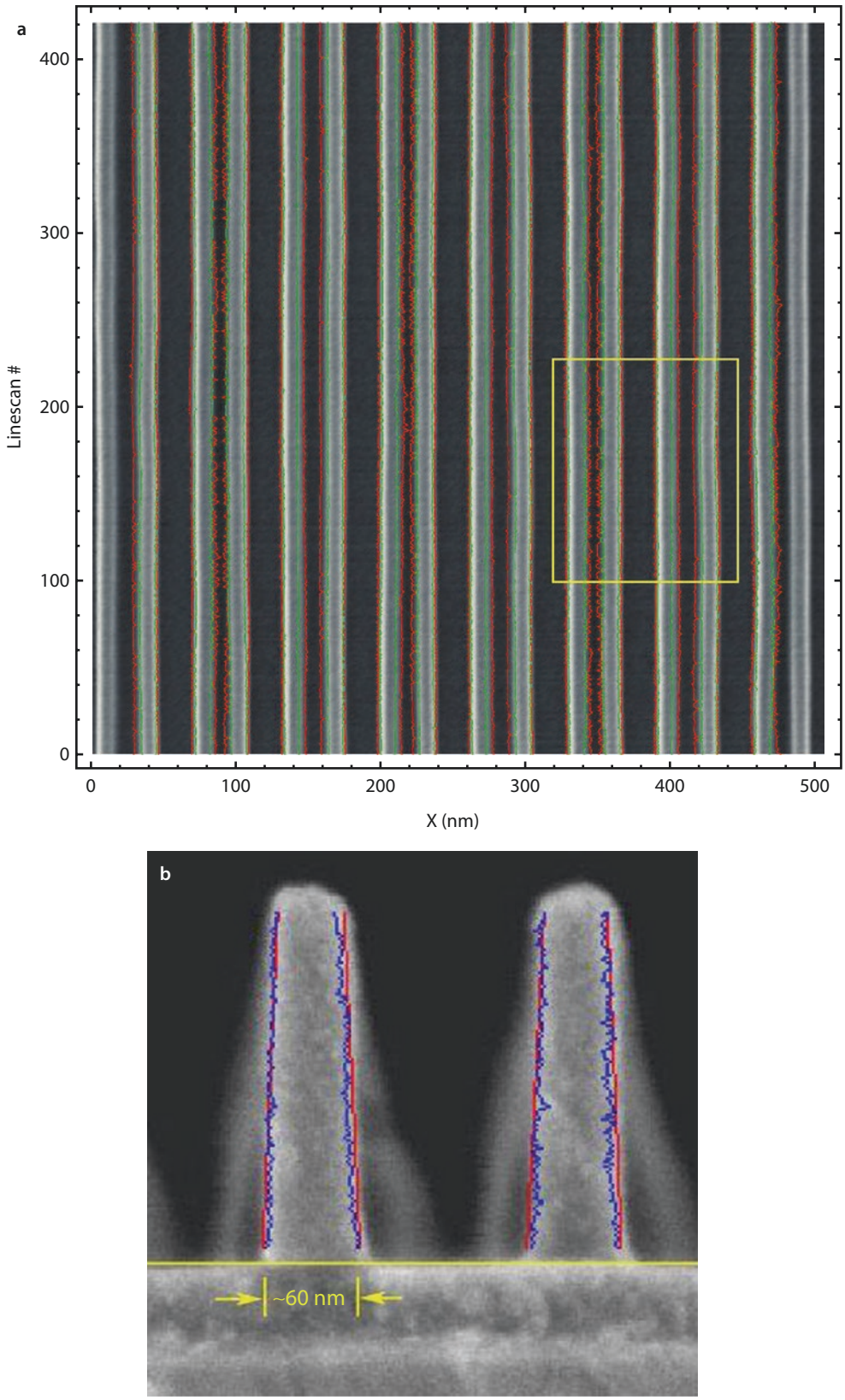

Fig. 10.10 **a** Top-down SEM image of line-width test structures; $E_0 = 15$ keV. **b** Side view of structures revealed by focused ion beam milling showing estimated shape from modeling of the top-down image (*red trace*) compared with the edges directly found in the cross sectional image (*blue*) (Villarrubia et al. 2015)

10.5 Achieving High Resolution with Secondary Electrons

Type 1 secondary electrons (SE_1), which are generated within the footprint of the incident beam and from the SE escape depth of a few nanometers, constitute an inherently high spatial resolution signal. SE_1 are capable of responding to specimen properties with lateral dimensions equal to the beam size as it is made progressively finer. Unfortunately, with the conventional Everhart–Thornley (positive bias) detector, the SE_1 are difficult to distinguish from the SE_2 and SE_3 signals which are created by the emerging BSEs, which effectively carry BSE information, and which are thus subject to the same long range spatial delocalization as BSEs. Strategies to improve high resolution imaging with SEs seek to modify the spatial characteristics and/or relative abundance of the SE_2 and SE_3 compared to the SE_1.

10.5.1 Beam Energy Strategies

Figure 10.11a shows schematically the narrow spatial distribution of the SE_1 emitted from a finely focused beam superimposed on the broader spatial distribution of the of the SE_2 and SE_3 that are created from the BSE distribution that would arise from a beam of intermediate energy, for example, 10 keV, on a material of intermediate atomic number, for example, Cu. While the beam can be focused to progressively smaller sizes within the limitations of the electron-optical system and the SE_1 will follow the beam footprint as it is reduced, the BSE-SE_2-SE_3 distributions remain at a fixed size defined by the extent of the interaction volume, which depends primarily on the composition and the beam energy and is insensitive to small beam size. For the situation shown in Fig. 10.11a, the SE_1 distribution can interact over a short spatial range with a feature that has dimensions similar to the focused beam footprint, but the extended BSE-SE_2-SE_3 distribution interacts with this feature over a longer range. The BSE-SE_2-SE_3 create a long, gradually decreasing signal tail, so that a sharp feature appears blurred. There are two different strategies for improving the resolution by choosing the beam energy at the extreme limits of the SEM range.

Low Beam Energy Strategy

As the beam energy is lowered, the electron range decreases rapidly, varying approximately as $E_0^{1.67}$. Since the BSE-SE_2-SE_3 distributions scale with the range, when the beam

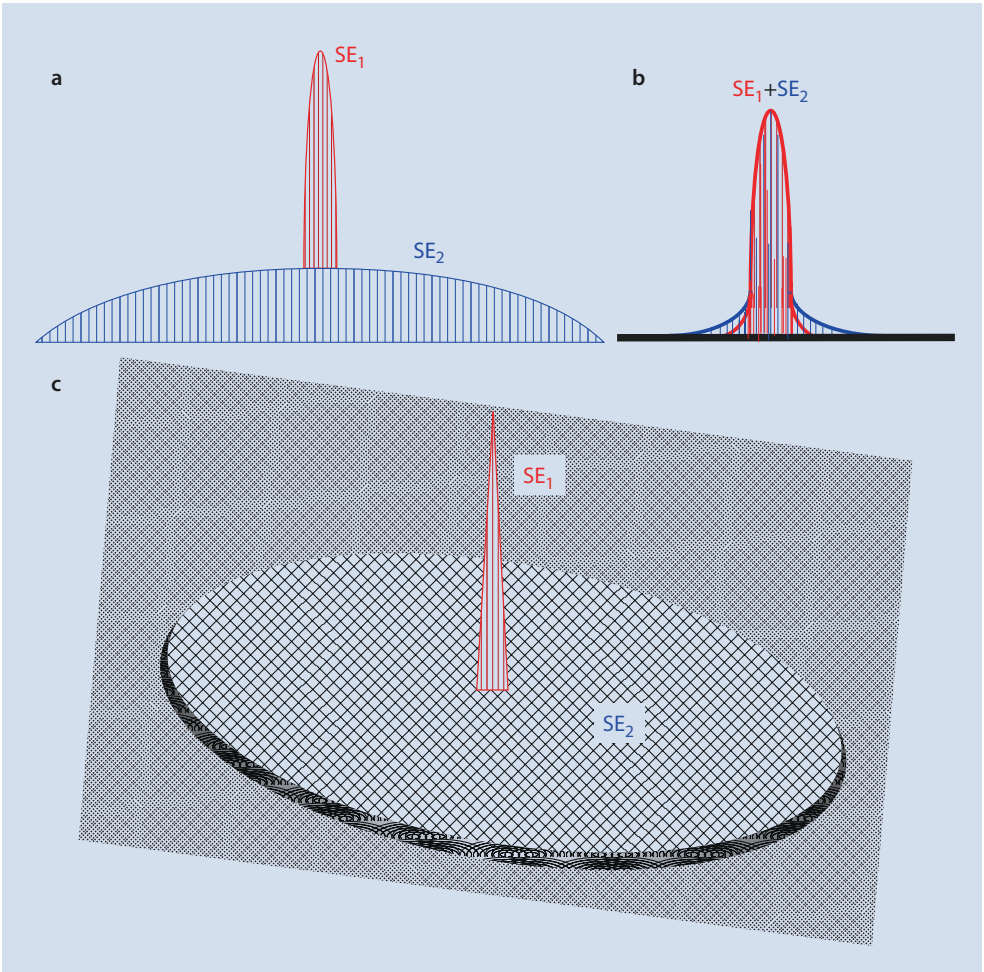

Fig. 10.11 **a** Schematic diagram of the SE_1 and SE_2 spatial distributions for an intermediate beam energy, e.g., $E_0 = 5–10$ keV. **b** Schematic diagram of the SE_1 and SE_2 spatial distributions for low beam energy, e.g., $E_0 = 1$ keV. **c** Schematic diagram of the SE_1 and SE_2 spatial distributions for high beam energy, e.g., $E_0 = 30$ keV

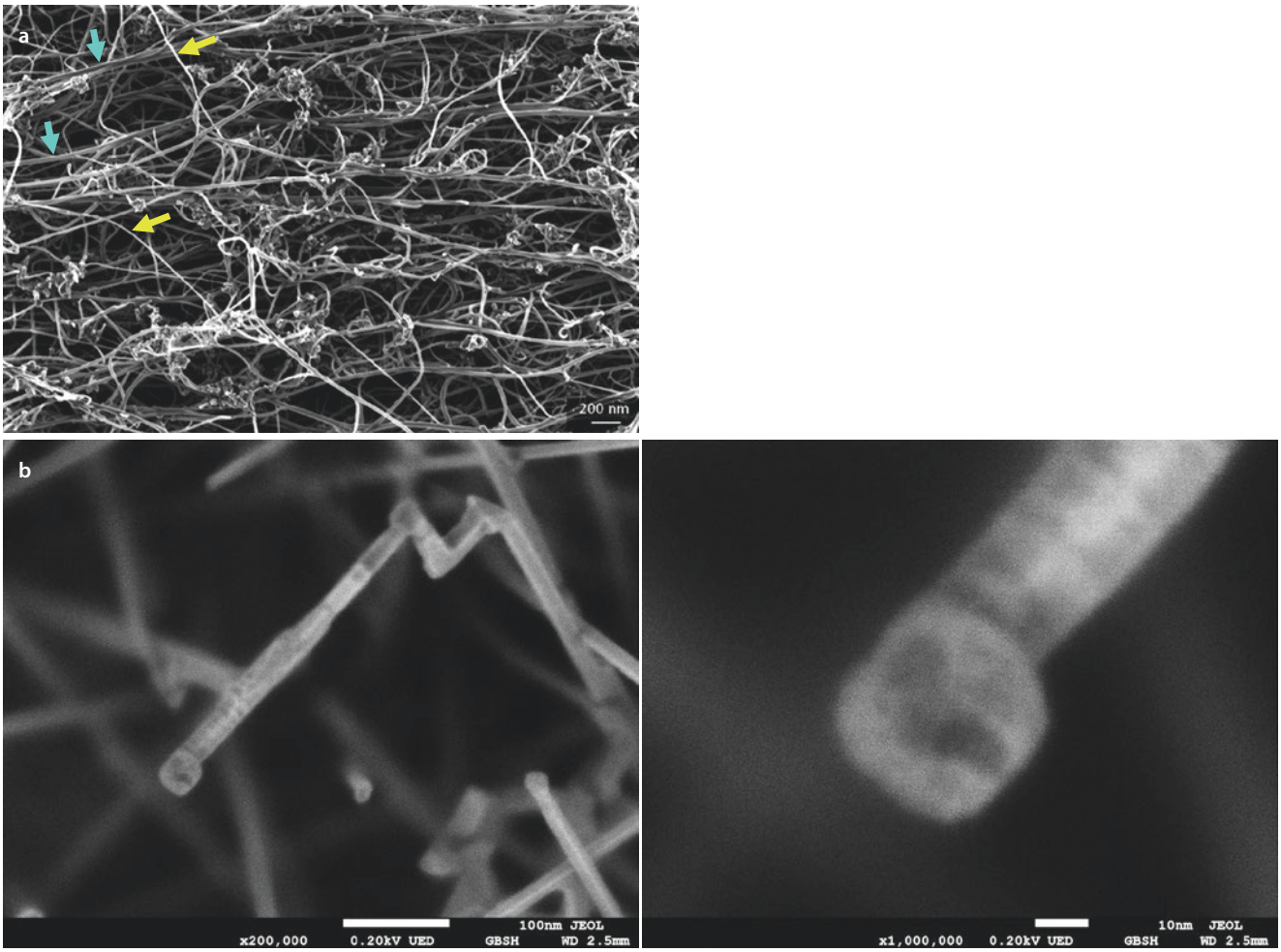

Fig. 10.12 **a** High resolution achieved at low beam energy, $E_0 = 1$ keV: image of carbon nanofibers. Note broad fibers (*cyan arrows*) with bright edges and darker interiors and thin fibers (*yellow arrows*) for which the bright edge effects converge (Bar = 200 nm) (Example courtesy John Notte, Zeiss). **b** High spatial resolution achieved at low landing energy: SnO_2 whisker imaged with a landing energy of 0.2 keV (left, Bar = 100 nm) (right, Bar = 10 nm) (Images courtesy V. Robertson, JEOL)

energy is reduced so that $E_0 \leq 2$ keV, the situation illustrated in Fig. 10.11b is reached for a finely focused beam (Joy 1984; Pawley 1984). The BSE-SE_2-SE_3 distributions collapse onto the SE_1 distribution, and all the signals now represent high spatial resolution information. An example of carbon nanofibers imaged at $E_0 = 1$ keV to achieve high resolution is shown in Fig. 10.12a. In Fig. 10.12a, the edges of the wider fibers appear bright (e.g., blue arrows) relative to the interior, as shown schematically in Fig. 10.7a. Figure 10.12 also illustrates the convergence of the bright edges of the narrow fibers (e.g., yellow arrows), as illustrated in Fig. 10.12b, to produce a very bright object against the background.

By applying a negative potential to the specimen, the landing energy can be reduced even further while preserving high spatial resolution, as shown in Fig. 10.12b for tin oxide whiskers imaged with a TTL SE detector at a landing energy of $E_0 = 0.2$ keV.

There are limitations of low beam energy operation that must be acknowledged (Pawley 1984). An inevitable consequence of low beam energy operation is the linear reduction in source brightness, which reduces the current that is contained in the focused probe which in turn affects feature visibility. Low energy beams are also more susceptible to interference from outside sources of electromagnetic radiation.

High Beam Energy Strategy

As the beam energy is increased, the electron range increases rapidly as $E_0^{1.67}$, broadening the spatial distribution of the BSE-SE_2-SE_3 signals while the SE_1 distribution remains fixed to the beam footprint. For example, when the beam energy is increased from 10 to 30 keV, the range increases by a factor of 6.3. With sufficient broadening, the spatial distributions of the BSE-SE_2-SE_3 signals do not significantly respond during beam scanning to small-scale features to which the SE_1 are sensitive. The BSE-SE_2-SE_3 signals then represent

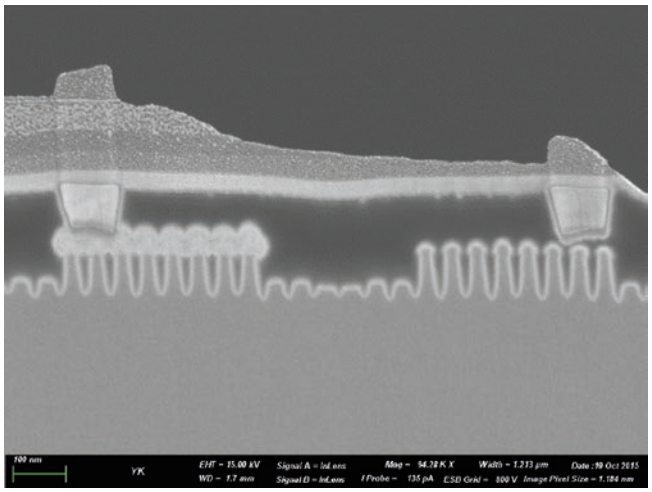

Fig. 10.13 High resolution achieved at high beam energy, $E_0 = 15$ keV: finFET transistor (16-nm technology) using the in lens SE detector in the Zeiss Auriga Cross beam. This cross section was prepared by inverted Ga FIB milling from backside (Bar = 100 nm) (Image courtesy of John Notte, Carl Zeiss)

a background noise component that, while it reduces the overall signal-to-noise, does not significantly alter the signal profiles across features. An advantage of operating at high beam energy is that the source brightness is increased, thus enabling more current to be obtained in a given focused probe size, which can help to compensate for the reduced signal-to-noise caused by the remote BSE-SE_2-SE_3 signals. An example of high beam energy imaging to achieve high resolution is shown in Fig. 10.13.

10.5.2 Improving the SE_1 Signal

Since the SE_1 Signal Is So Critical To Achieving High Resolution, What Can Be Done To Improve It?

Excluding the SE_3 Component

For a bulk specimen, the high resolution SE_1 component only forms 5–20 % of the total SE signal collected by the E–T(positive bias) detector, while the lower resolution SE_2 and SE_3 components of roughly similar strength form the majority of the SE signal. While the SE_1 and SE_2 components are generated within 1 to 10 µm, the SE_3 are produced millimeters to centimeters away from the specimen when the BSEs strike instrument components. This substantial physical separation is exploited by the class of "through-the-lens" (TTL) detectors, which utilize the strong magnetic field of the objective lens to capture the SE_1 and SE_2 which travel up the bore of the lens and are accelerated onto a scintillator-photomultiplier detector. Virtually all of the SE_3 are excluded by their points of origin being outside of the lens magnetic field. For an SE_1 component of 10 % and SE_2 and SE_3 components of 45 %, the ratio of high resolution/low resolution signals thus changes from 0.1 for the E–T(positive bias) detector to 0.22 for the TTL detector.

Making More SE_1: Apply a Thin High-δ Metal Coating

Because SEs are generated within a thin surface layer, the SE coefficient δ of the first few atomic layers will dominate the SE emission of the specimen. For specimens that consist of elements such as carbon with a low value of δ, the SE_1 signal can be increased by applying a thin coating (one to a few nanometers) of a high SE emitter such as gold-palladium (rather than pure gold, which deposits as islands that can be mistaken for specimen structure), or platinum-family metals. While such a coating can also serve to dissipate charging from an insulating specimen, even for conducting carbonaceous materials the heavy-metal coating increases the surface SE_1 emission of the specimen while not significantly increasing the scattering of beam electrons due to its minimal thickness so that BSE, SE_2, and SE_3 signals are not affected. As shown schematically in Fig. 10.14a, the SE signal across an uncoated particle shows an increase at the edge due to the grazing beam incidence, but after a thin high-δ metal coating

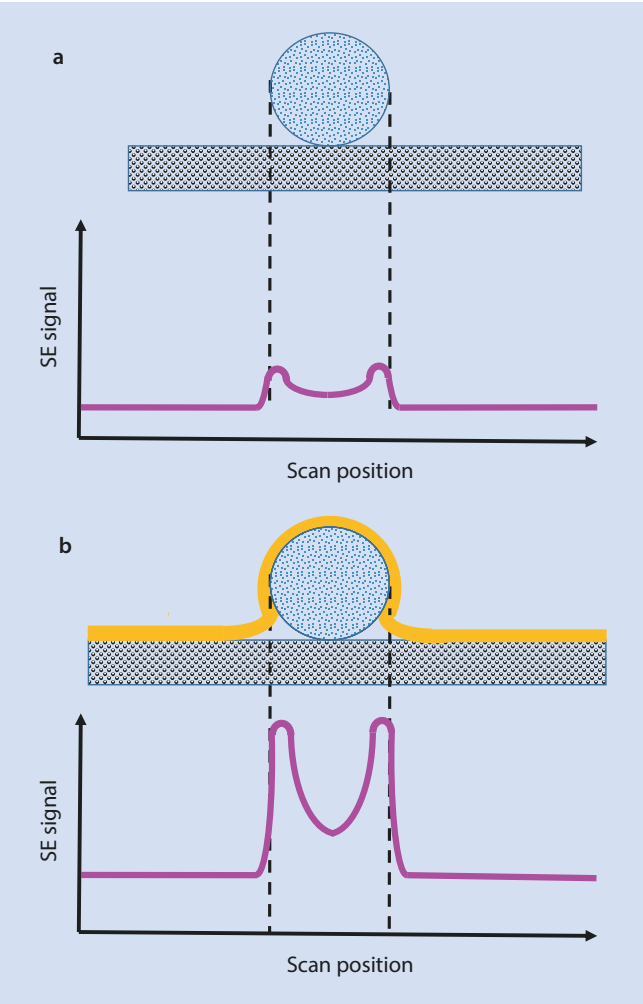

Fig. 10.14 Schematic illustration of the effect of heavy metal, high δ coating to increase contrast from low-Z targets: **a** SE signal trace from an uncoated particle; **b** signal trace after coating with thin Au-Pd

is applied (Fig. 10.14b), the SE signal at the edges of features will be substantially enhanced.

Making Fewer BSEs, SE_2, and SE_3 by Eliminating Bulk Scattering From the Substrate

For the important class of specimens such as nanoscale particles which have such small mass thickness that the beam electrons penetrate through the particle into the underlying bulk substrate, the large BSE, SE_2 and SE_3 components that dominates the E–T(positive bias) signal respond to substrate properties and don't actually represent specimen information at all. Thus, the high resolution imaging situation can be significantly improved by eliminating the bulk substrate. The particles are deposited on an ultrathin (~10-nm) carbon film supported on a metal (Cu, Ni, etc.) grid. This grid is placed over a deep blind hole drilled in a block of carbon that will serve as a Faraday cup for the beam electrons that pass though the particles, as shown schematically in Fig. 10.15a. An example of this preparation is shown for particles of SRM470

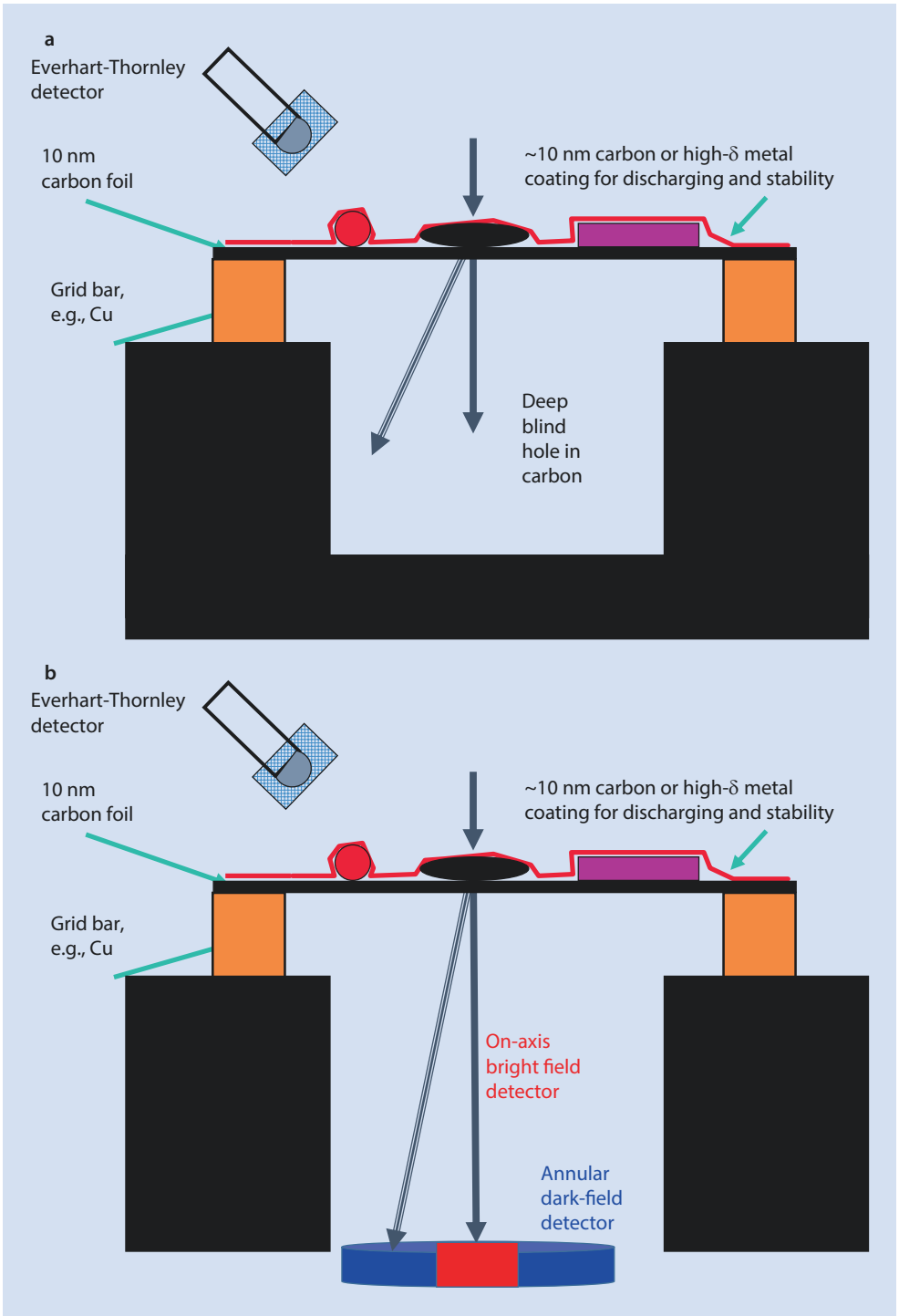

Fig. 10.15 **a** Schematic illustration of specimen mounting strategy to minimize background by eliminating the bulk substrate. **b** Scanning transmission electron microscopy (STEM) two component detector for high energy electrons: on-axis bright-field detector and surrounding annular dark-field detector

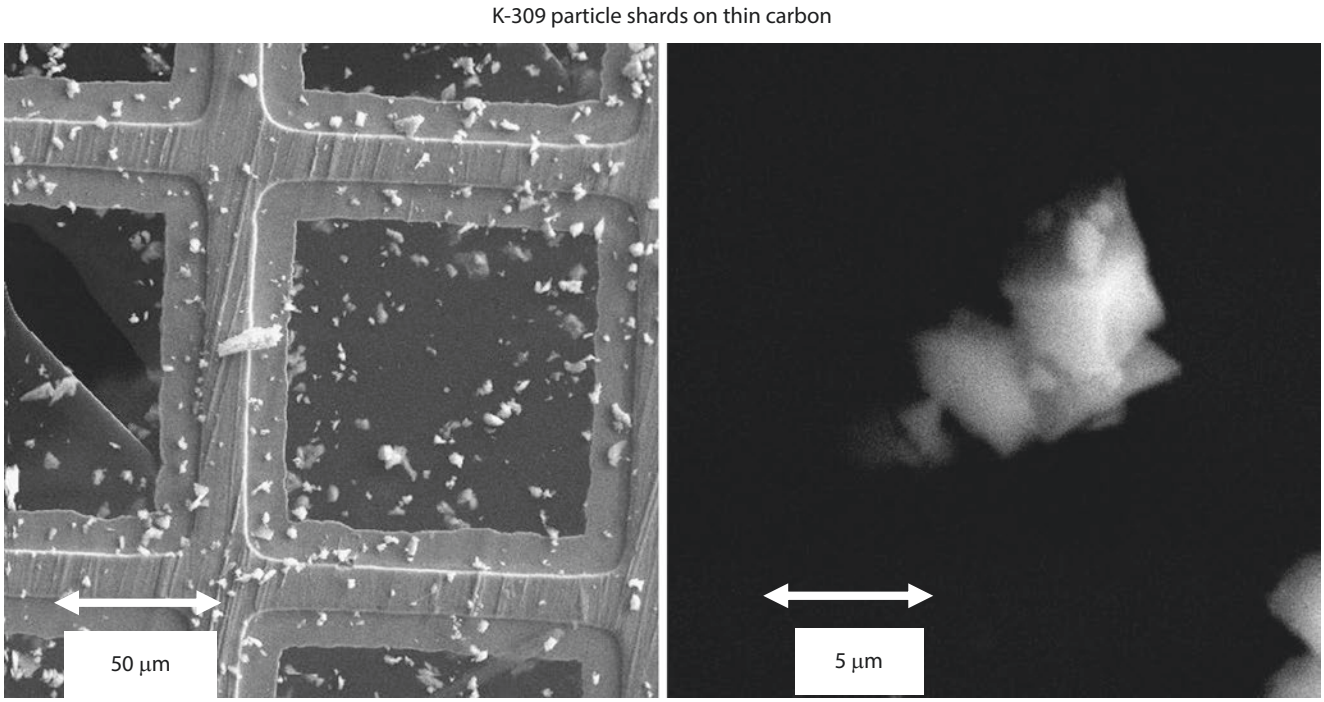

Fig. 10.16 SEM imaging glass shards deposited on a thin (~ 10-nm carbon) at $E_0 = 20$ keV and placed over a deep blind hole in a carbon block

(K411 glass) in Fig. 10.16. By selecting operation at the highest beam energy available, for example, 20–30 keV, backscattering will be minimized along with the SE_2 and SE_3 signals.

Scanning Transmission Electron Microscopy in the Scanning Electron Microscope (STEM-in-SEM)

The "thin film" support method for nanoscale particles and other thin specimens (either inherently thin or prepared as thin sections by ion beam milling) can be further exploited by collecting the beam electrons that transmit through the specimen to create a scanning transmission electron microscope (STEM) image, as illustrated in Fig. 10.15b. To create the STEM image, an appropriate detector, such as a passive scintillator-photomultiplier, is placed below the specimen grid on the optical axis. The size of this detector is such that it accepts only electrons traveling close to the optical axis that pass through the specimen unscattered. Those electrons that experience even a small angle elastic scattering event that causes an angular deviation of a few degrees will miss the detector. Thus, the regions of the specimen with minimal scattering will appear bright, while those with sufficient mass to cause elastic scattering will appear dark, creating a "bright-field" image. A more elaborate STEM detector array can include an annular ring detector co-mounted with the central on-axis bright-field detector to capture the elastically scattered transmitted electrons from the specimen, as illustrated in Fig. 10.15b. This off-axis annular detector produces a "dark-field" image since the thin regions such as the support film that do not produce significant scattering events will appear dark. Portions of the specimen that do scatter sufficiently will appear bright. Since elastic scattering depends strongly on local atomic number, compositional effects can be observed in the dark field STEM image. An example of a high resolution STEM-in-SEM image created with an annular off-axis detector is shown in Fig. 10.17.

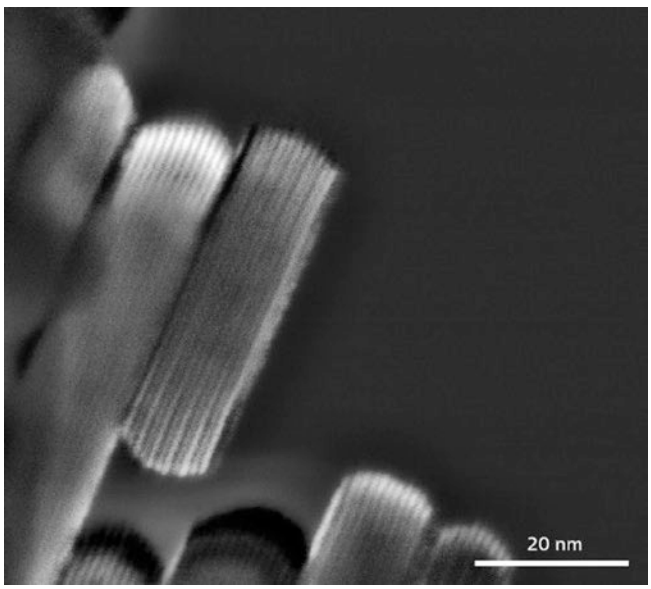

Fig. 10.17 Dark-field annular detector STEM image of $BaFe_{12}O_{19}$ nanoparticles; $E_0 = 22$ keV using oriented dark-field detector in the Zeiss Gemini SEM. The 1.1-nm (002) lattice spacing is clearly evident (Image courtesy of John Notte, Carl Zeiss. Image processed with ImageJ-Fiji CLAHE function)

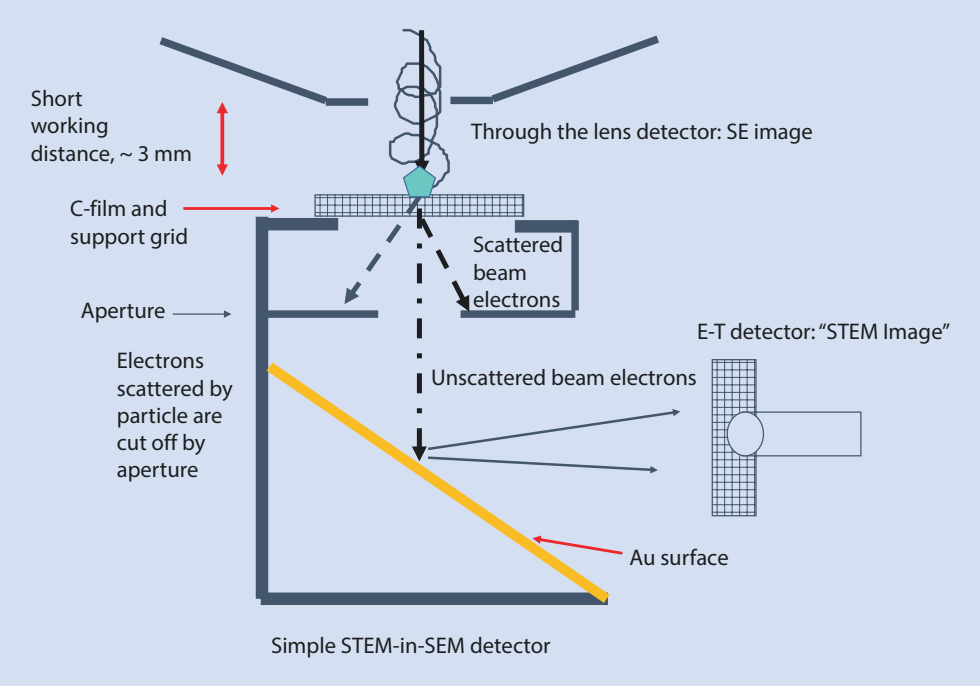

Fig. 10.18 Schematic cross section of a STEM-in-SEM detector that makes use of the Everhart–Thornley(positive bias) detector to form a bright-field STEM image

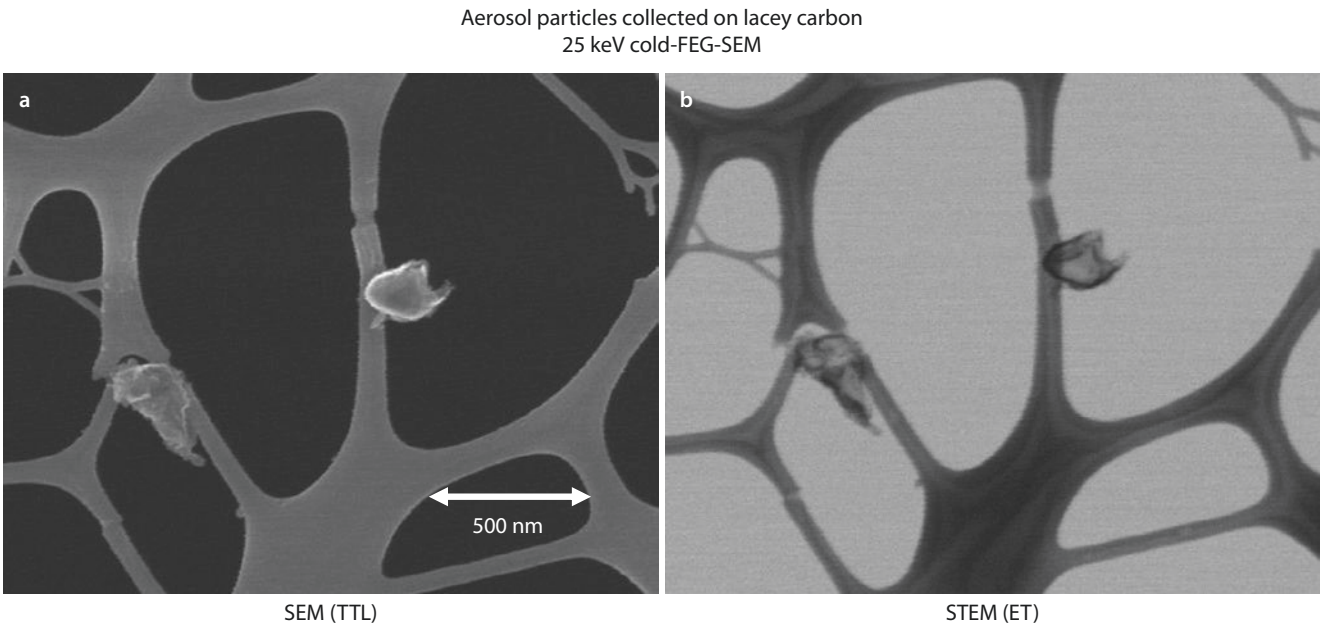

Fig. 10.19 Aerosol contamination particles deposited on lacey-carbon film and simultaneously imaged with a TTL detector for SE_1 and the STEM-in-SEM detector shown in Fig. 10.18 (Example courtesy John Small, NIST)

A simple STEM-in-SEM bright-field detector can be created as shown in Fig. 10.18. The grid carrying the thin specimen is placed over an aperture that serves to stop electrons that have suffered an elastic scattering event in the specimen. The unscattered beam electrons pass through this aperture and strike a gold-covered surface below, where they generate strong SE emission, which is then attracted to the E–T(positive bias) detector, creating a bright-field image. If the SEM is also equipped with a TTL detector, the nearly pure SE_1 image that arises from a thin specimen can be collected with the TTL detector simultaneously with the bright-field STEM image collected with the E–T(positive bias) detector, as shown for particles supported on a lacey-carbon film in Fig. 10.19.

10.5.3 Eliminate the Use of SEs Altogether: "Low Loss BSEs"

BSEs are usually considered a low resolution signal because of the substantial delocalization that results from multiple elastic scattering of the beam electrons at conventional beam

energy, for example, $E_0 \geq 10$ keV. However, high resolution SEM can be achieved by eliminating the use of SEs as the imaging signal and instead relying on the BSEs, specifically those that have lost very little of the initial beam energy. Because of the energy loss due to inelastic scattering that occurs for high energy beam electrons at a nearly constant rate, dE/ds, with distance traveled in the specimen, low loss BSEs represent beam electrons that have emerged from the specimen after traveling very short paths through the specimen. These low loss electrons are thus sensitive to specimen scattering properties very close to the entrance beam footprint and from a very shallow surface region, thus constituting a high resolution signal. Wells (1974a, b) first demonstrated the utility of this approach by using an energy filter to select the "low loss" backscattered electrons (LL BSE) that had lost less than a specified fraction, for example, 5 %, of the initial beam energy. At normal beam incidence, the LL BSE fraction of the total BSE population is very low, and their trajectories are spread over a wide angular range, the 2π azimuth around the beam, making their efficient collection difficult. The population of LL BSE can be increased, and their angular spread greatly decreased, by tilting the specimen to a high angle, for example, 70° or higher. As shown schematically in Fig. 10.20, at this tilt angle a single elastic scattering event greater than 20°, which also has a suitable azimuthal angular component along the trajectory, can carry the beam electron out of the specimen as a low loss BSE after traveling along a short path within the specimen. The energy filter with an applied potential V + ΔV then serves to decelerate and exclude BSEs that have lost more than a specified ΔE of the incident energy. Since the electrons that pass through the filter have been retarded to a low kinetic energy, the detector following the filter must include an acceleration field, such as that of the Everhart–Thornley detector, to raise the kinetic energy to a detectable level for detection.

An example comparing TTL SE and LL BSE (10 % energy window) images of etched photoresist at low beam energy ($E_0 = 2$ keV) is shown in Fig. 10.21 (Postek et al. 2001). Note the enhanced surface detail visible on the top of the resist pattern in the LL BSE image compared to the SE image. The extreme directionality of the LL BSE detector leads to loss of signal on surfaces not tilted toward the detector, resulting in

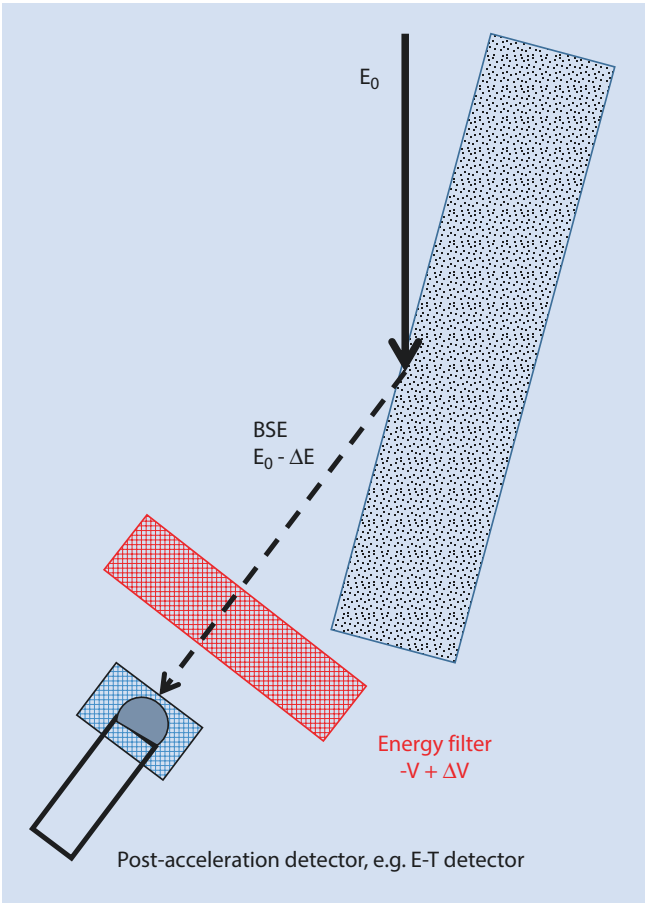

Fig. 10.20 Schematic illustration of low loss BSE imaging from a highly tilted specimen using an energy filter

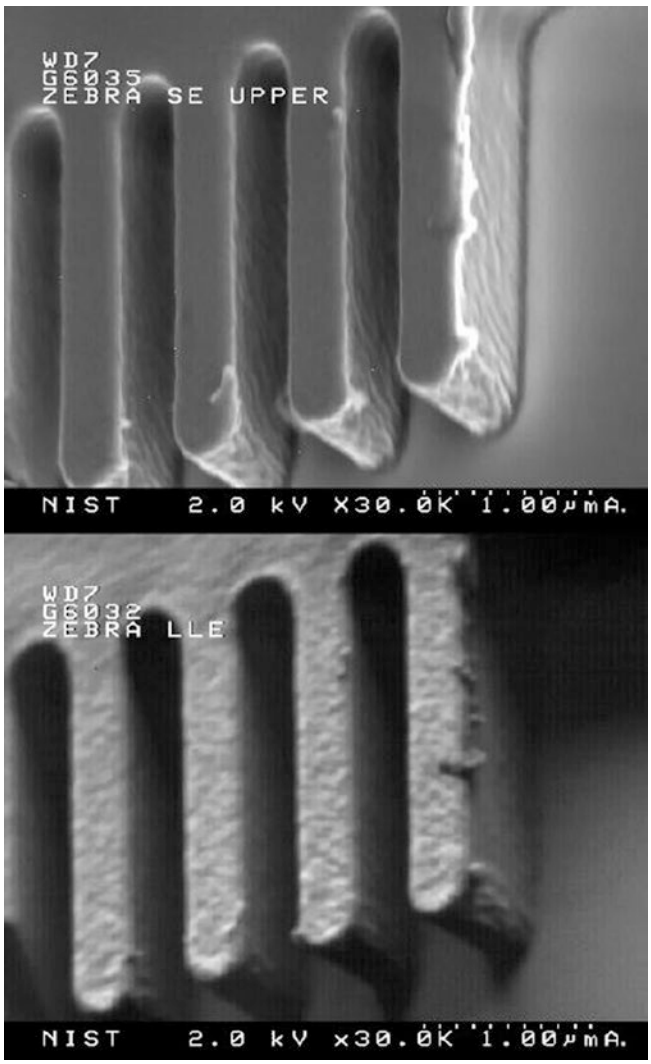

Fig. 10.21 SE (*upper*) and low loss BSE (*lower*) images of photoresist at $E_0 = 2$ keV. Note the enhanced detail visible on the surface of the LL-BSE image compared to the SE image (Postek et al. 2001)

poor signal collection on the sides of the steps, which are illuminated in the TTL SE detector image.

While the example in Fig. 10.21 illustrates the utility of LL BSE imaging at low beam energy, LL BSE imaging also enables operation of the SEM at high beam energy (Wells 1971), thus maximizing the electron gun brightness to enable a small beam with maximum current. Low loss images provide both high lateral spatial resolution and a shallow sampling depth.

10.6 Factors That Hinder Achieving High Resolution

10.6.1 Achieving Visibility: The Threshold Contrast

High resolution SEM involves working with a finely focused beam which even when optimized to minimize the effects of aberrations inevitably carries a small current, often as low as a few picoamperes, because of the restrictions imposed by the Brightness Equation. The inevitable consequence of operating with low beam current is the problem of establishing the visibility of the features of interest because of the restrictions imposed by the Threshold Equation. For a given selection of operating parameters, including beam current, detector solid angle, signal conversion efficiency, and pixel dwell time, there is always a threshold of detectable contrast. Features producing contrast below this threshold contrast will not be visible at the pixel density selected for the scan, even with post-processing of the image with various advanced image manipulation algorithms. It is important to understand that a major consequence of the Threshold Equation is that the absence of a feature in an SEM image is not a guarantee of the absence of that feature on the specimen: the feature may not be producing sufficient contrast to exceed the threshold contrast for the particular operating conditions chosen. Because of the action of the "bright edge effect" in high resolution SE images to produce very high contrast, approaching unity, between the edges of a feature and its interior, the ready visibility of the edges of features, while obviously useful and important, can give a false sense of security with regard to the absence of topographic details within the bulk of a feature. In fact, those weaker topographic features may be producing contrast that is below the threshold of visibility. To perform "due diligence" and explore the possibility of features lurking below the threshold of visibility, the threshold contrast must be lowered:

$$i_B > \frac{\left(4\times10^{-18}\right)N_{PE}}{(\eta,\delta)DQEC^2t_F}\left(\text{coulomb}/s=\text{amperes}\right) \quad (10.4)$$

where N_{PE} is the number of pixels in the image scan, η and δ are the backscatter or secondary electron coefficients as appropriate to the signal selected, DQE is the detective quantum efficiency, which includes the solid angle of collection for the electrons of interest and the conversion into detected signal, C is the contrast that the feature produces, and t_F is the frame time. Equation 10.4 reveals the constraints the microscopist faces: if the beam current is determined by the requirement to maintain a certain beam size and the detector has been optimized for the signal(s) that the features of interest are likely to produce, then the only factor remaining to manipulate to lower the threshold contrast is to extend the dwell time per pixel (t_F/N_{PE}). While using longer pixel dwell times is certainly an important strategy that should be exploited, other factors may limit its utility, including specimen drift, contamination, and damage due to increased dose. Thus, performing high resolution SEM almost always a dynamic tension when establishing the visibility of low contrast features between the electron dose needed to exceed the threshold of visibility and the consequences of that electron dose to the specimen.

10.6.2 Pathological Specimen Behavior

The electron dose needed for high resolution SEM even with an optimized instrument can exceed the radiation damage threshold for certain materials, especially "soft" materials such as biological materials and other weakly bonded organic and inorganic substances. Damage may be readily apparent in repeated scans, especially when the magnification is lowered after recording an image. If such specimen damage is severe, a "minimum-dose" strategy may be necessary, including such procedures as focusing and optimizing the image on a nearby area, blanking the beam, translating the specimen to an unexposed area, and then exposing the specimen for a single imaging frame.

Another possibility is to explore the sensitivity of the specimen to damage over a wide range of beam energy. It may seem likely that operating at low beam energy should minimize specimen damage, but this may not be the case. Because the electron range scales as $E_0^{1.67}$ and the volume as $(E_0^{1.67})^3$ while the energy deposited scales as E_0, the energy deposited per unit volume scales roughly as

$$\text{Energy / unit volume} = E_0 / \left(E_0^{1.67}\right)^3 = 1/E_0^4 \quad (10.5)$$

Thus, increasing the beam energy from 1 to 10 keV lowers the energy deposited per unit volume by a factor of approximately 10,000. This simplistic argument obviously ignores the substantial variation in the energy density within the interaction volume as well as the possibility that some damage mechanisms have an energy threshold for activation that may be avoided by lowering the beam energy. Nevertheless, Eq. 10.5 suggests that examining the material susceptibility to damage over a wide range of beam energy may be a useful strategy.

10.6.3 Pathological Specimen and Instrumentation Behavior

Contamination

A modern SEM that is well maintained should not be the source of any contamination that is observed. The first requirement of avoiding contamination is a specimen preparation protocol that minimizes the incorporation of or retention of contaminating compounds when processing the specimen. This caution includes the specimen as well as the mounting materials such as sticky conductive tape. A specimen airlock that minimizes the volume brought to atmosphere for specimen exchange as well as providing the important capability of pre-pumping the specimen to remove volatile compounds prior to insertion in the specimen chamber is an important capability for high resolution SEM. The specimen airlock can also be equipped with a "plasma cleaner" that generates a low energy oxygen ion stream for destruction and removal of organic compounds that produce contamination. If contamination is still observed after a careful preparation and insertion protocol has been followed, it is much more likely that the source of contamination remains the specimen itself and not the SEM vacuum system.

Instabilities

Unstable imaging conditions can arise from several sources. (1) Drift and vibration: The specimen preparation, the method of attachment to the substrate, the attachment of the specimen mount to the stage, and the stage itself must all have high stability to avoid drift, which is most noticeable at high magnification, and isolation from sources of vibration. Note that some mounting materials such as sticky tape may be subject to beam damage and distortion when struck by the beam electrons, leading to significant drift. One of the most stable mechanical stage designs is to be mounted within the bore of the objective lens, although such designs severely limit the size of the specimen and the extent of lateral motion that can be achieved. (2) Electromagnetic radiation interference: A periodic distortion is sometimes observed that is a result of interference from various sources of electromagnetic radiation, including emissions from 60-Hz AC sources, including emissions from fluorescent lighting fixtures. Rather than being random, this type of interference can synchronize with the scan and can be recorded. An example of this type of image defect is shown in Fig. 10.22. Eliminating this type of interference and the resulting image defects can be extremely challenging.

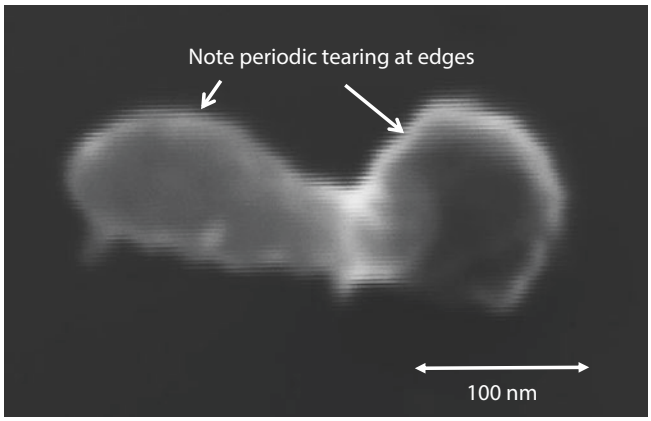

Fig. 10.22 SEM image of nanoparticles showing tearing at the particle edges caused by some source of electromagnetic interference whose frequency is constant and apparently locked to the 60 Hz AC power

References

Joy DC (1984) Beam interactions, contrast and resolution in the SEM. J Microsc 136:241

Oatley CW (1972) The scanning electron microscope, part 1, the instrument. Cambridge University Press, Cambridge

Pawley JB (1984) Low voltage scanning electron microscopy. J Microsc 136:45

Peters K-R (1984) Generation, collection, and properties of an SE-1 enriched signal suitable for high resolution SEM on bulk specimens. In: Kyser DF, Niedrig H, Newbury DE, Shimizu R (eds) Electron beam interactions with solids for microscopy, microanalysis, and microlithography. SEM, Inc, AMF O'Hare, p 363

Peters K-R (1985) "Working at higher magnifications in scanning electron microscopy with secondary and backscattered electrons on metal coated biological specimens" SEM/1985. SEM, Inc, AMF O'Hare, p 1519

Postek MT, Vladar AE, Wells OC, Lowney JL (2001) Application of the low-loss scanning electron microscope image to integrated circuit technology. Part 1 – applications to accurate dimension measurements. Scanning 23:298

Villarrubia J, Vladar A, Ming B, Kline R, Sunday D, Chawla J, List S (2015) Scanning electron microscope measurement of width and shape of 10 nm patterned lines using a JMONSEL-modeled library. Ultramicroscopy 154:15–28

Wells OC (1971) Low-loss image for surface scanning electron microscopy. Appl Phys Lett 19:232

Wells OC (1974a) Scanning electron microscopy. McGraw-Hill, New York

Wells OC (1974b) Resolution of the topographic image in the SEM. SEM/1974. IIT Research Inst, Chicago, p 1